

Evidence of structural transition and spin-lattice coupling in antiferromagnetic $MnSi_2Te_4$

Z Y Pang(庞兆宇), K Liao(了可), S J Zhang(张圣杰), Rao Fei(费饶), Cui Zhang(张萃), Richeng Yu(禹日成), Gang Wang(王刚), Sheng Meng(孟胜), and Jimin Zhao(赵继民)
Citation: Chin. Phys. B, 2026, 35 (**8**): 087401. DOI: 10.1088/1674-1056/ae64d5
http://cpb.iphy.ac.cn; http://iopscience.iop.org/cpb

What follows is a list of articles you may be interested in

Synergistic SERS effects in organic/MoS_2 heterojunctions with cavity structure enabling nanoplastics screening and antibiotic adsorption behavior detection

Liqi Ma(马立琪), Abdur Rahim(阿卜杜勒-拉希姆), Baiju Lü(吕白菊), Muhammad Saleem(穆罕默德-萨利姆), Xiaoyu Zhang(张晓雨), Mingyue Li(李明月), Muhammad Zahid(穆罕默德-扎希德), and Mei Liu(刘玫)
Chin. Phys. B, 2025, 34 (**4**): 047402. DOI: 10.1088/1674-1056/ada888

SERS activity of carbon nanotubes modified by silver nanoparticles with different particle sizes

Xiao-Lei Zhang(张晓蕾), Jie Zhang(张洁), Yuan Luo(罗元), and Jia Ran(冉佳)
Chin. Phys. B, 2022, 31 (**7**): 077401. DOI: 10.1088/1674-1056/ac4f51

Raman phonon anomalies in $Sr(Fe_{1-x}Co_x)_2As_2$

Yanxing Yang(杨彦兴), Hewei Zhang(张鹤巍), and Haizheng Zhuang(庄海正)
Chin. Phys. B, 2022, 31 (**2**): 027401. DOI: 10.1088/1674-1056/ac0cd6

Highly sensitive and stable SERS probes of alternately deposited Ag and Au layers on 3D SiO_2 nanogrids for detection of trace mercury ions

Yi Tian(田毅), Han-Fu Wang(王汉夫), Lan-Qin Yan(闫兰琴), Xian-Feng Zhang(张先锋), Attia Falak, Pei-Pei Chen(陈佩佩), Feng-Liang Dong(董凤良), Lian-Feng Sun(孙连峰), Wei-Guo Chu(褚卫国)
Chin. Phys. B, 2018, 27 (**7**): 077406. DOI: 10.1088/1674-1056/27/7/077406

High-pressure synchrotron x-ray diffraction and Raman spectroscopic study of plumbogummite

Duan Kang(康端), Xiang Wu(巫翔), Guan Yuan(袁冠), Sheng-Xuan Huang(黄圣轩), Jing-Jing Niu(牛菁菁), Jing Gao(高静), Shan Qin(秦善)
Chin. Phys. B, 2018, 27 (**1**): 017402. DOI: 10.1088/1674-1056/27/1/017402

Evidence of structural transition and spin–lattice coupling in antiferromagnetic $MnSi_2Te_4$

Z Y Pang(庞兆宇)[1,2,†], K Liao(了可)[1,2,†], S J Zhang(张圣杰)[1,†], Rao Fei(费饶)[1,2,†], Cui Zhang(张萃)[1,2], Richeng Yu(禹日成)[1,2], Gang Wang(王刚)[1], Sheng Meng(孟胜)[1,2,3,‡], and Jimin Zhao(赵继民)[1,2,3,§]

[1] *Beijing National Laboratory for Condensed Matter Physics, Institute of Physics, Chinese Academy of Sciences, Beijing* 100190, *China*
[2] *School of Physical Sciences, University of Chinese Academy of Sciences, Beijing* 100049, *China*
[3] *Songshan Lake Materials Laboratory, Dongguan* 523808, *China*

(Received 15 March 2026; revised manuscript received 19 April 2026; accepted manuscript online 27 April 2026)

Layered van der Waals magnetic chalcogenides provide an important platform for exploring the interplay between lattice dynamics and magnetic correlations in low-dimensional systems. Here, we present a comprehensive temperature-dependent Raman spectroscopy study of a layered antiferromagnetic semiconductor $MnSi_2Te_4$, which exhibits large negative magnetoresistance. Several Raman modes exhibit pronounced and mode-selective anomalies in frequency, linewidth, and intensity near the antiferromagnetic Néel temperature (18.6 K) and a possible hidden phase transition temperature (100 K), whereby deviations from Curie–Weiss behavior in magnetic susceptibility were previously reported. Angle-resolved polarized Raman spectroscopy (ARPRS) measurements reveal distinct polarization-dependent responses for different Raman modes. These results indicate a nontrivial coupling between lattice vibrations and magnetic ordering in $MnSi_2Te_4$, and demonstrate Raman spectroscopy as an effective probe of structural phase transition and spin–lattice coupling in van der Waals magnets.

Keywords: Raman scattering, structural phase transition, transition metal chalcogenides, phonon

PACS: 74.25.nd, 78.30.–j, 64.70.Nd, 74.70.Xa, 63.20.–e

DOI: 10.1088/1674-1056/ae64d5 **CSTR:** 32038.14.CPB.ae64d5

1. Introduction

Layered magnetic chalcogenides have attracted extensive attention in recent years owing to their rich magnetic ground states and strong coupling between lattice, spin, and electronic degrees of freedom.[1–5] In these systems, reduced dimensionality and competing exchange interactions often give rise to complex magnetic behavior, including multiple magnetic transitions, short-range magnetic correlations well above the long-range ordering temperature, and pronounced anisotropy in physical properties.[6–9] Understanding how the lattice responds to and interacts with such magnetic phenomena is essential for elucidating the microscopic mechanisms governing their collective behavior.

$MnSi_2Te_4$ is a layered van der Waals antiferromagnetic semiconductor, with a collinear G-type antiferromagnetic ground state and a Néel temperature T_N at 18.6 K.[10] Its layered crystal structure and well-defined magnetic order make it a representative system for investigating lattice dynamics in van der Waals magnets, crystallizes in a triclinic space group $P\bar{1}$ (No. 2). The sample growth method is detailed in the supporting information (SI). Magnetic susceptibility measurements[10] reveal deviations from Curie–Weiss behavior at temperatures far above T_N, extending to approximately 100 K, suggesting additional magnetic correlations beyond the long-range ordered state. However, the microscopic origin of these anomalies, particularly the possible involvement of lattice degrees of freedom, remains unexplored.

Raman spectroscopy is a powerful, symmetry-sensitive probe of lattice vibrations and has proven particularly effective in revealing interactions between phonons and other degrees of freedom,[9,11–18] such as charge,[19–21] orbital,[22] and spin.[23] In magnetic materials, deviations of phonon frequencies, linewidths, or intensities from conventional anharmonic behavior are often indicative of spin–phonon coupling, arising from the modulation of magnetic exchange interactions by lattice vibrations.[24–27] Furthermore, angle-resolved polarized Raman spectroscopy (ARPRS) provides additional insight into phonon symmetries and in-plane anisotropy, enabling reliable identification of vibrational anisotropy and polarization-dependent effects that may accompany magnetic or structural crossovers.[28–31]

In this work, we present a comprehensive temperature-dependent Raman and ARPRS study of $MnSi_2Te_4$ over a wide temperature range from 7.5 K to 293 K. Several phonon modes exhibit anomalous behavior in frequency, linewidth, and intensity, with clear signatures. Our results reveal both spin–lattice

[†]These authors contributed equally to this work.
[‡]Corresponding author. E-mail: smeng@iphy.ac.cn
[§]Corresponding author. E-mail: jmzhao@iphy.ac.cn

© 2026 Chinese Physical Society and IOP Publishing Ltd. All rights, including for text and data mining, AI training, and similar technologies, are reserved.

coupling and a structural phase transition in the layered large negative magnetoresistance material $MnSi_2Te_4$.

2. Experiment and analysis

2.1. Temperature dependent Raman spectroscopy

Temperature-dependent Raman measurements were performed using a SmartRaman confocal micro-Raman system (designed and made by the Institute of Semiconductors, Chinese Academy of Sciences) equipped with a $\times 50$ objective in a backscattering geometry. The system was coupled to a Horiba iHR-550 spectrometer with an 1800 grooves/mm diffraction grating and a liquid nitrogen-cooled charge coupled device detector, of which the overall spectral resolution for Raman scattering is 3.3 cm^{-1}. A 532 nm laser was used as the excitation source with an incident power of 0.425 mW. For temperature-dependent Raman measurements, a neutral density filter with an optical density (OD) of 2.0 was applied to minimize laser-induced heating effects on the lattice, whereas an OD of 1.0 was used for the ARPRS measurements. Raman spectra were collected in the range of 70 cm^{-1} to 400 cm^{-1}. To exclude possible photoluminescence contributions, additional Raman measurements were performed at 293 K using a 633 nm excitation wavelength, and the spectra obtained with 532 nm and 633 nm excitations were compared.

Low-temperature Raman measurements were carried out using a liquid helium cooled LT-3OM cryostat with a temperature stability of ± 0.1 K. Spectra were recorded over a temperature range from 7.5 K to 293 K, covering the antiferromagnetic transition at 18.6 K. Temperature-dependent measurements were conducted during a controlled heating cycle.

2.2. Angle-resolved polarized Raman spectroscopy

ARPRS measurements were carried out by rotating the polarization of both the incident and scattered light while keeping the sample stationary. Polarization control was achieved by inserting half-wave plates into the confocal optical paths of the excitation and collection channels. In this configuration, the relative polarization angle was varied continuously over a full 360° rotation without changing the laser spot position on the sample and was measured at every 10°. All ARPRS measurements were performed in a parallel polarization configuration, where the polarization direction of the incident laser beam was kept parallel to that of the scattered light.[3,32]

2.3. Density functional theory calculations

First-principles calculations were performed based on density functional theory (DFT) methods implemented in the Quantum Espresso package.[33] The exchange–correlation interaction was treated using the Perdew–Burke–Ernzerhof functional within the generalized gradient approximation.[34] The electronic wave functions were expanded in plane waves with a kinetic energy cutoff of 500 eV. Brillouin zone integrations were carried out using a Monkhorst–Pack k-point mesh of $12 \times 12 \times 6$. All the atoms were fully relaxed until the forces on each atom were less than 0.001 eV/Å.

3. Results and discussion

Figure 1(a) shows the polarization configuration for angle-resolved polarized Raman spectroscopy. Figure 1(b) shows the Raman spectrum of $MnSi_2Te_4$ measured at 7.5 K. Several well-resolved Raman peaks are observed in the low-frequency range, reflecting the rich lattice dynamics of this layered ternary chalcogenide. The clearly separated peaks allow reliable peak fitting and quantitative extraction of peak position, linewidth, and intensity, forming the basis of the temperature-dependent analysis.

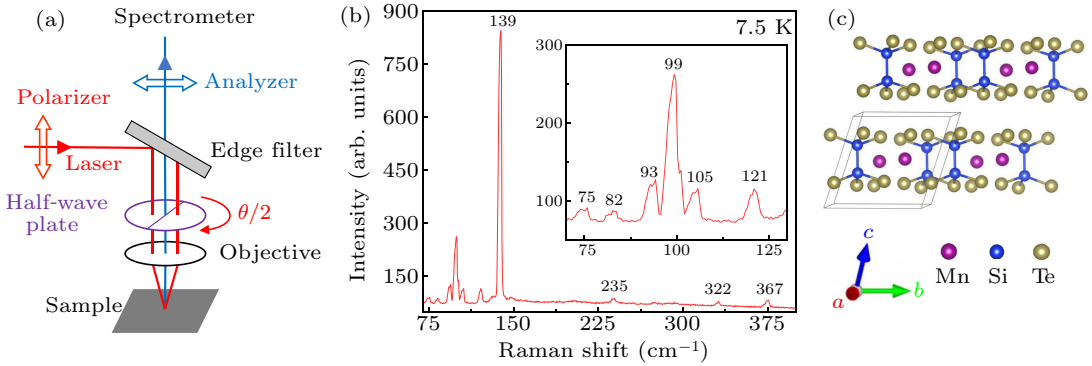


Fig. 1. (a) Schematic experimental setup for angle-resolved polarized Raman spectroscopy. (b) Raman spectrum of $MnSi_2Te_4$ measured at 7.5 K. (c) Crystal structure of $MnSi_2Te_4$; the primitive cell is indicated by the black frame.[10] Corresponding vibrational modes are shown in Fig. S1 of the supporting information.

The crystal structure of $MnSi_2Te_4$ is illustrated in Fig. 1(c). $MnSi_2Te_4$ crystallizes in a layered van der Waals structure composed of alternating [$MnTe_6$] and [Si_2Te_6] octahedra, which stack along the crystallographic c axis. Within each layer, the octahedra are arranged in a zigzag pattern, resulting in a low-symmetry intralayer structure.[10]

Figure 2 presents the Raman spectra of $MnSi_2Te_4$ measured at 293 K under excitations with 532 nm and 633 nm

laser beams. The nearly identical Raman peak values obtained with the two excitation wavelengths are identical to each other, demonstrating that the observed features originate from Raman scattering rather than photoluminescence.

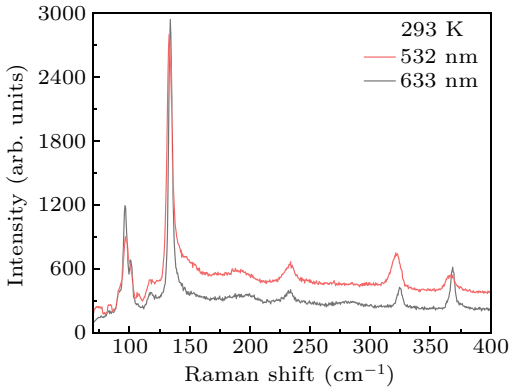


Fig. 2. Raman spectra of $MnSi_2Te_4$ measured at 293 K, excited with 532 nm and 633 nm lasers, respectively.

Figure 3 presents the temperature-dependent evolution of $MnSi_2Te_4$ Raman peaks measured from 7.5 K to 293 K. The overall Raman intensity gradually decreases with increasing temperature, accompanied by progressive peak broadening, consistent with enhanced phonon–phonon scattering at elevated temperatures.[3] To quantify the temperature-dependent behavior, selected Raman peaks at 93 cm^{-1}, 99 cm^{-1}, 105 cm^{-1}, 121 cm^{-1}, and 139 cm^{-1} are fitted using Gaussian line shapes, and the extracted peak positions, full widths at half maximum (FWHM), and intensities are summarized in Figs. 3(b)–3(d). These peaks exhibit distinct temperature dependence, indicating a mode-selective lattice response rather than an overall thermal effect.

The temperature dependence of the Raman peak frequencies reveals two characteristic transitions. For Raman peaks at 93 cm^{-1}, 105 cm^{-1}, and 139 cm^{-1}, the positions remain nearly constant at low temperatures and begin to shift more rapidly upon increasing temperature. A change in slope is observed near T_N at 18.6 K, followed by a more pronounced deviation from a smooth trend, disappearing above 100 K. Such behavior deviates from a simple anharmonic phonon model and suggests the presence of further contributions to the phonon renormalization, indicating the existence of a structural phase transition.[23,24,35–37]

The Raman intensities in Fig. 3(b) also display nontrivial temperature dependences.[38–40] While the intensity of peaks at 93 cm^{-1} and 139 cm^{-1} shows a monotonic decrease with increasing temperature, others (99 cm^{-1}, 105 cm^{-1}, and 121 cm^{-1}) exhibit pronounced anomalies. In particular, the mode at 105 cm^{-1} shows a pronounced maximum near T_N (18.6 K). These anomalies are mode-selective, suggesting that the coupling strength sensitively depends on the phonon modes. Such a variation in lattice degrees of freedom occurring upon a magnetic phase transition reveals that there is a coupling between the lattice vibration and long-range magnetic ordering in $MnSi_2Te_4$. Thus, it indicates there is spin–lattice coupling in $MnSi_2Te_4$.[41]

The FWHM analysis reinforces this observation. Although a gradual linewidth broadening with temperature is expected due to anharmonic phonon–phonon scattering,[37,42] all modes at 93–139 cm^{-1} exhibit deviations from this behavior (Figs. 3(c) and 3(d)), including non-monotonic linewidth changes or an onset of broadening at temperatures that is consistent with the anomalies observed in phonon frequency and intensity.

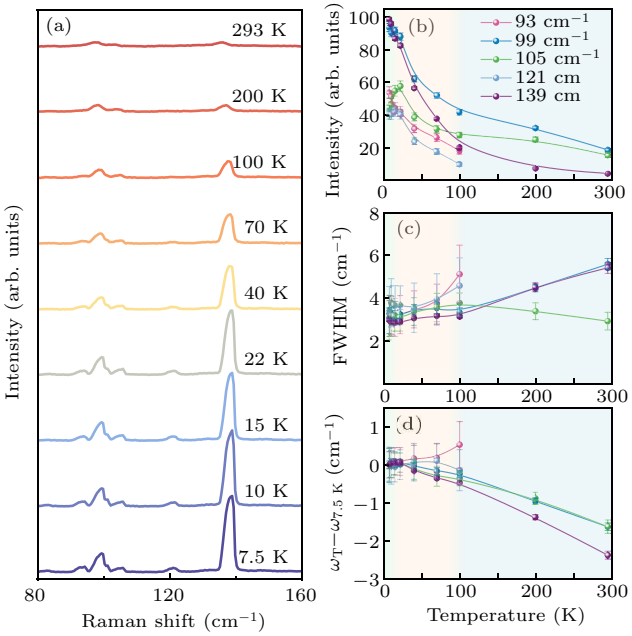


Fig. 3. (a) Temperature-dependent Raman spectra of $MnSi_2Te_4$ (see Fig. S2 in the supporting information for additional temperature-dependent spectra). Temperature evolution of the (b) intensity, (c) FWHM, and (d) peak positions for selected Raman modes. Colored backgrounds: different phase regions. For clarity, the intensities of 99 cm^{-1} and 139 cm^{-1} are linearly scaled down.

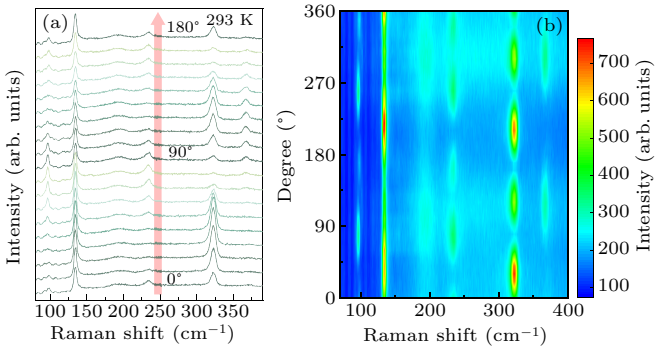


Fig. 4. ARPRS of $MnSi_2Te_4$ measured at 293 K with a 10° step. (a) Polarization-resolved Raman spectra measured from 0° to 180°. For completeness, polarization-resolved Raman spectra from 0° to 360° are provided in Fig. S3 of the supporting information. (b) Two-dimensional ARPRS intensity map.

Notably, the distinct phonon behavior at the higher temperature 100 K is clearly consistent with the deviation from the Curie–Weiss behavior in magnetic susceptibility.[10,11] Thus, we interpret this consistency as revealing a lattice change of

$MnSi_2Te_4$, which exists well above the long-range antiferromagnetic ordering temperature. Consequently, we attribute this to a structural phase transition in $MnSi_2Te_4$.

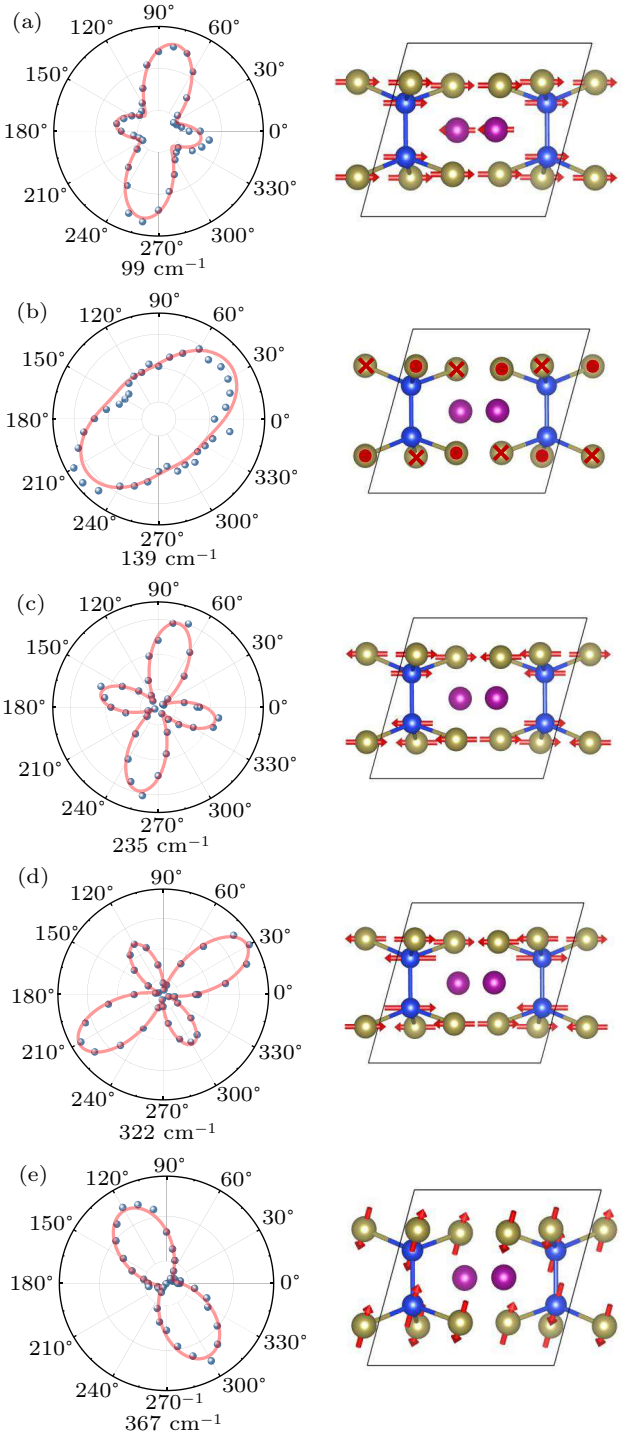


Fig. 5. Polar plots of the ARPRS intensity and corresponding atomic displacement patterns for representative phonon modes of $MnSi_2Te_4$: (a) 99 cm^{-1}, (b) 139 cm^{-1}, (c) 235 cm^{-1}, (d) 322 cm^{-1}, and (e) 367 cm^{-1}. The directions of atomic vibrations are denoted with red arrows, while out-of-plane vibrational components are denoted by red dots and crosses, representing atomic displacements pointing out of and into the plane, respectively.

Figure 4 presents the ARPRS intensity map of $MnSi_2Te_4$, showing the evolution of Raman intensity as a function of both Raman shift and polarization angle. Distinct angular modulation is observed for different Raman peaks, indicating a mode-specific polarization dependence.[43,44] Figures 5(a)–5(e) show the polar plots of the Raman intensity for representative modes at 99 cm^{-1}, 139 cm^{-1}, 235 cm^{-1}, 322 cm^{-1}, and 367 cm^{-1}. Each mode exhibits a characteristic angular dependence with a distinct modulation pattern and periodicity.[45] While modes at 139 cm^{-1} and 367 cm^{-1} display relatively smooth and sinusoidal variations, others (99 cm^{-1}, 235 cm^{-1}, and 322 cm^{-1}) show more complex angular profiles with multiple intensity maxima and minima within a 360° rotation. The angular modulation observed for different Raman modes indicates that the measured Raman response reflects intrinsic crystalline symmetry, rather than extrinsic effects such as sample misalignment or polarization leakage.

DFT calculations provide a microscopic reference for the vibrational frequencies and polarization trends observed in the low-temperature Raman and ARPRS measurements. As summarized in Table 1, the calculated phonon frequencies are in good agreement with the experimentally observed Raman peaks. The DFT phonon calculations correspond to the harmonic vibrational frequencies at the 0 K equilibrium structure, making them directly comparable to low-temperature Raman spectra. Beyond the frequency scale, the vibrational eigenmodes obtained from DFT capture the essential features of the polarization-dependent Raman response. Raman modes at 99 cm^{-1}, 235 cm^{-1}, and 322 cm^{-1} exhibit pronounced angular modulation in the *ab* plane, giving rise to characteristic four-lobe polarization patterns, reflecting the in-plane anisotropy of their vibrational character. In contrast, modes at 139 cm^{-1} and 367 cm^{-1} display smoother elliptical angular dependences, consistent with vibrational eigenmodes that involve substantial out-of-plane atomic displacements. The qualitative agreement between experimentally observed ARPRS patterns and theoretical polarization trends well explains the origin of the mode-selective polarization behavior in $MnSi_2Te_4$.

Table 1. Experimental and theoretical Raman peak positions (cm^{-1}).

Experiment	82	93	99	99	105	121	139	235	322	367
DFT	79.9	90.2	99.8	100.2	110.0	125.4	141.6	251.7	350.2	367.4

4. Conclusion

In summary, we have performed systematic temperature-dependent Raman scattering and angle-resolved polarized Raman spectroscopy studies on a layered van der Waals antiferromagnetic semiconductor $MnSi_2Te_4$. Several phonon modes exhibit temperature-dependent anomalies in frequency, linewidth, and intensity appearing near $T_N = 18.6$ K and around 100 K, in line with the deviation from Curie–Weiss behavior in magnetic susceptibility. Our ARPRS measurements reveal distinct polarization-dependent responses, whose

anisotropy is determined by the lattice symmetry. Consequently, our Raman spectroscopy investigation reveals both a structural phase transition and spin–lattice coupling in van der Waals $MnSi_2Te_4$.

Data availability statement

The data that support the findings of this study are openly available in Science Data Bank at https://doi.org/10.57760/sciencedb.j00113.00324.

Acknowledgements

This work was financially supported by the National Key Research and Development Program of China (Grant Nos. 2024YFA1408700 and 2021YFA1400201), the National Natural Science Foundation of China (Grant Nos. 52325201, 12534006, and 12025407), the CAS Project for Young Scientists in Basic Research (Grant Nos. YSBR-059 and YSBR-047), International Partnership Program of Chinese Academy of Sciences (Grant No. GJHZ1826), and CAS Interdisciplinary Innovation Team.

References

[1] Qiu J, Huang W J, Lee Y J, Kim S, Chen X B and Yang I S 2024 *Results in Physics* **56** 107256
[2] Wang P, Zhu S C, Zou Y T, Wang P, Zhu S C, Zou Y T, Chen H Y, Liu Y, Li W W, Chen J, Zhu J L, Wu L S, Wang S M, Yang W G, Xiao Y M, Chow P, Wang L P and Zhao Y S 2022 *Chem. Mater.* **34** 3931
[3] Zhang X, Tan Q H, Wu J B, Shi W and Tan P H 2016 *Nanoscale* **8** 6435
[4] Wu Q, Zhou H X, Wu Y L, Hu L L, Ni S L, Tian Y C, Sun F, Zhou F, Dong X L, Zhao Z X and Zhao J M 2020 *Chin. Phys. Lett.* **37** 097802
[5] Jiazila H, Wu Y L, Shi M Z, Zhai Y N, Wu Q, Liu Z, Zhou Y, Chen X H and Zhao J M 2025 *Proc. Natl. Acad. Sci. USA* **122** e2406464122
[6] Gao T, Zhang Q, Li L, Zhou X, Li L G, Li H Q and Zhai T Y 2018 *Adv. Optical Mater.* **6** 1800058
[7] Li T S, Luo W J, Kitadai H, Wang X Z and Ling X 2019 *Adv. Mater.* **31** 1807160
[8] Jiang X, Liu Q L, Xing J P, Liu N S, Guo Y, Liu Z F and Zhao J J 2021 *Appl. Phys. Rev.* **8** 031305
[9] Zhang X, Qiao X F, Shi W, Wu J B, Jiang D S and Tan P H 2015 *Chem. Soc. Rev.* **44** 2757
[10] Liao K, Yin B, Pan Y, Chen L, Liu C, Do S H, Gao Y F, Yang Y L, Wang Y L, Wang X H, Li Y, Guo Z N, Liu J W, Wang J O, Su D, Ma J, Wu Q S and Wang G 2026 *J. Am. Chem. Soc.* **148** 340
[11] Ji J T, Zhang A M, Yang R, Tian Y, Jin F, Qiu X G and Zhang Q M 2016 *Chin. Phys. B* **25** 067803
[12] Loudon R 1964 *Adv. Phys.* **13** 423
[13] Pawbake A S, Island J O, Flores E, Ares J R, Sanchez C, Ferrer I J, Jadkar S R, Herr S J, Andres C G and Dattatray J L 2015 *Appl. Mater. Interfaces* **7** 24185
[14] Raman C V and Krishnan K S 1928 *Nature* **121** 501
[15] Devereaux T P and Hackl R 2007 *Rev. Mod. Phys.* **79** 175
[16] Ma H, Li L W and Bi X Y, *et al.* 2025 *The Journal of Light Scattering* **37** 357
[17] Hasaien J, Shan P F, Zhou F R and Zhao J M 2025 *Rev. Sci. Instrum.* **96** 013004
[18] Zhai Y N, Gong P M, Hasaien J, Zhou F R and Zhao J M 2024 *Progress in Surface Science* **99** 100761
[19] Singh A, Elsukova A, Rawat D, Talukdar S, Saha S, le Febvrier A, Persson POA, Eklund P and Soni A 2025 *Phys. Rev. B* **111** 195203
[20] Wu Y L, Yin X, Hasaien J, Ding Y and Zhao J M 2020 *Chin. Phys. Lett.* **37** 047801
[21] Sun F, Wang R, Aku-Leh C, Yang H X, He R and Zhao J M 2014 *Scientific Reports* **4** 6429
[22] Pal S, Seth A, Ali A, Singh Y, Muthu D V S, Bhattacharjee S and Sood A K 2023 *Phys. Rev. B* **108** L241103
[23] Chandra S, Kaur G, Gupta R, Chakravarty S, Bhalerao G M and Govindaraj R 2024 *Phys. Scr.* **99** 095910
[24] Zhang J, Peng Z P, Soni A, Zhao Y Y, Xiong Y, Peng B, Wang J B, Dresselhaus M S and Xiong Q H 2011 *Nano Lett.* **11** 2407
[25] Kotnana G, Sathe V G and Narayana J S 2018 *J. Raman Spectrosc.* **49** 764
[26] Wu Y L, Yu X H, Hasaien J, Hong F, Shan P F, Tian Z Y, Zhai Y N, Hu J P, Cheng J G and Zhao J M 2024 *Nat. Commun.* **15** 9683
[27] Lin X N, Fu S H, Zhai Y N, Wang W H, Li H C, Zhang R Z, Meng S and Zhao J M 2024 *The Innovations* **5** 100614
[28] Liu X L, Zhang X, Lin M L and Tan P H 2017 *Chin. Phys. B* **26** 067802
[29] Yoon D, Moon H, Son Y W, Samsonidze G, Park B H, Kim J B, Lee Y and Cheong H 2008 *Nano Lett.* **8** 4270
[30] Kim J, Lee J U and Cheong H 2020 *J. Phys.: Condens. Matter* **32** 343001
[31] Liu J Y, Zhang L L, Wang Z Y, Zhao M M, Wu B B, Long H D, Chang X, Tao Y, Du M H, Wang Y B, Wang Z G and Lei L 2025 *Appl. Phys. Lett.* **127** 213103
[32] Schaack G 2000 *Raman Scattering by Crystal-Field Excitations*, in Light Scattering in Solids VII. Topics in Applied Physics Vol. 75 pp. 24–173
[33] Giannozzi P, Baroni S and Bonini N, *et al.* 2009 *J. Phys.: Condens. Matter* **21** 395502
[34] Perdew J P, Burke K and Ernzerhof M 1997 *Phys. Rev. Lett.* **78** 1396
[35] Cheng Y, Zhou F R, Teng J, Li P Y, Jiang L T, Gong P M, Li Y Q, Wu X J, Kartner F X and Zhao J M 2025 *Nat. Commun.* **16** 5656
[36] Bagchi S, Poweleit C D, Beeler R T, Kouvetakis J and Menendez J 2011 *Phys. Rev. B* **84** 193201
[37] Balkanski M, Wallis R F and Haro E 1983 *Phys. Rev. B* **28** 1928
[38] Mishra K K, Sivasubramanian V and Arora A K 2011 *Raman Spectrosc.* **42** 517
[39] Sonika, Singh Y and Yadav C S 2022 *J. Alloys Compd.* **897** 163220
[40] Mączka M, Sanjuán M L, Fuentes A F, Hermanowicz K and Hanuza J 2008 *Phys. Rev. B* **78** 134420
[41] Hu L L, Yang M, Wu Y L, Wu Q, Zhaol H, Sun F, Wang W, He R, He S L, Zhang H, Huang R J, Li L F, Shi Y G and Zhao J M 2019 *Phys. Rev. B* **99** 094307
[42] Tang H and Herman I P 1991 *Phys. Rev. B* **43** 2299
[43] Mao N N, Wu J X, Han B W, Lin J J, Tong L M and Zhang J 2016 *Small* **12** 2627
[44] Kranert C, Sturm C, Schmidt-Grund R and Grundmann M 2016 *Phys. Rev. Lett.* **116** 127401
[45] Nguyen M H, Son S, Park G, Na W K, Park J G and Cheong H 2024 *J. Mater. Chem. C* **12** 12468